STM JOURNALS

Journal of
Polymer & Composites

ISSN: 2321-2810 (Online)
ISSN: 2321-8525 (Print)
Volume 13, Special Issue 1, 2025
DOI (Journal): 10.37591/JoPC

https://journals.stmjournals.com/jopc

Research JoPC

A Comparative Study on Formaldehyde Detection Capabilities in Pristine Graphene and Ag-doped Graphene Sheet

Indranil Maity[1,*], Souvik Bhanja[2], Soubarno Chatterjee[2]

Abstract

The present work concerns a detailed investigation of the enhanced formaldehyde (also known as methanal) detection by decorating the pristine (or bare) graphene nanosheet with silver (Ag) nano-particle (or foreign Ag atom). The bare graphene sheet was exposed to the formaldehyde vapor forming the formaldehyde-adsorbed pristine graphene sheet (taken as Case-I), and whose results were studied and compared with the outcomes obtained from the formaldehyde-adsorbed Ag-decorated graphene sheet (taken as Case-II). The design and modeling of the nanocomposites were derived through the Density Functional Theory (DFT) study, which was performed on the Gaussian 09W (for calculation purposes) and Gauss View 6.0 (for visualization purposes) platforms. The Highest Occupied Molecular Orbital (HOMO), and the Lowest Unoccupied Molecular Orbital (LUMO) have been analyzed along with their corresponding energy values to find the HOMO-LUMO gap for both Case-I, and Case-II. Adsorption energy was found to be stronger upon the introduction of Ag atom as a dopant into the graphene sheet. The charge density of the systems in Case-I and Case-II were revealed from the Electrostatic Potential (ESP) map, which provided information about the electron richness or deficiency of the surfaces. The band structure, plotted using the Materials Studio package, provided an insight into the semi-metallic nature of both Case-I and Case-II nanostructures. It was noticed that the binding distance between the formaldehyde and the graphene sheet got shortened in the case of Ag-decorated graphene. The above observations clearly infer that Ag-decorated graphene is a better alternative to pristine graphene for formaldehyde detection.

Keywords: Ag-decorated hybrid nanostructures, graphene based smart nanocomposites, modeling and simulation methodologies, high-performance sensing application, formaldehyde adsorption

***Author for Correspondence**
Indranil Maity
Email: indrasanu026@gmail.com

[1]Assistant Professor, Department of Electronics and Communication Engineering (ECE), Institute of Engineering and Management (IEM), University of Engineering and Management (UEM), Kolkata, West Bengal, India
[2]Student, Department of Electronics and Communication Engineering (ECE), Institute of Engineering and Management (IEM), Kolkata, West Bengal, India

Received Date: July 26, 2024
Accepted Date: October 05, 2024
Published Date: November 20, 2024

Citation: Indranil Maity, Souvik Bhanja, Soubarno Chatterjee. A Comparative Study on Formaldehyde Detection Capabilities in Pristine Graphene and Ag-doped Graphene Sheet. Journal of Polymer & Composites. 2025; 13(Special Issue 1): S801-S809p.

INTRODUCTION

Formaldehyde (HCHO) is the simplest organic compound that can be formed by incorporating the carbonyl functional group (C=O). It is a flammable gas at room temperature, characterized by its colourless and foul-smelling nature [1-2]. Formaldehyde is most widely used in industries to form resins for wooden products. It can be utilized as a disinfectant, fungicide and germicide. It also finds its use in the medical field as an antiseptic. It is a popular embalming agent for preserving human and animal remains [2-3]. However, the downside of this useful compound is that it is a pollutant whose high concentration in the human body can cause rare cancers [2-4]. So, proper monitoring of formaldehyde levels (i.e., one of the crucial volatile organic compounds: VOCs), would contribute

towards biomedical applications. That is why, the development of new measuring device is necessary for an effective and accurate detection of formaldehyde present into the atmosphere.

Graphene sheet, a lightweight, 2D lattice of carbon atoms, is an emerging and smart nanomaterial that has garnered significant curiosity due to its remarkable properties [5]. Researchers explore its potential usage in solid-state gas sensors owing to its exceptional material properties like substantial surface area, high electrical and thermal conductivity, low resistivity and low thermal noise. However, the agglomeration, chemical inertness, buckling and sp^2 hybridization in bare graphene restrict its use in certain fields [6-7]. To address these bottlenecks, chemical modification of pristine graphene surface has been done by doping with novel element like Ag-atom. Ag-doping gets rid of the sp^2 hybridization and alters its band gap in a way to enhance reactivity and also improves gas-sensing and catalytic behaviour [6].

Singh et al. examined the glucose adsorption probability of graphene by using Au (gold), Ni (nickel), Cu (copper), Pt (platinum) and Ag atoms as surface dopants and also studied their corresponding stability, sensitivity, conductivity, and response time [7]. Zhang et al. further studied about the sensitiveness of the Ag-decorated graphene sheet for the decomposition products of SF_6 (sulfur hexafluoride) [8]. Different transition metals were employed via doping in a graphene sheet by Yang et al. to find out the potential metal for sensing formaldehyde that established the fact that Ag, Cu, Co (cobalt), Pd (palladium), Ni, Zn (zinc) are comparatively more capable than other transition metal [9]. Li et al. made a comparison between different gases (nitrogen dioxide, methane, carbon dioxide, ammonia, water, and ethane) on Ag-substituted graphene sheet and concluded that nitrogen dioxide is the most susceptible to adsorption [10]. Singla et al. studied the hydrogen gas detection mechanism of pristine and Ag-decorated graphene via DFT calculation [11].

This study focuses on figuring out which nanomaterial-based gas-sensor has better detection capabilities between the pristine graphene and Ag-doped graphene when exposed to formaldehyde gas/vapor by investigating the sensing mechanisms. First principle calculations have been used to obtain the geometrically valid structures of Case-I and Case-II based on which different electronic properties like HOMO-LUMO, ESP, DOS (Density of States), band structure and Mulliken charge were derived and discussed along with their significance. Additionally, an in-depth comparison was made between Case-I and Case-II highlighting their adsorption energies and binding distances, which has not been reported by any submitted work so far, as per our knowledge.

MATERIALS AND METHODS

The investigation was carried out on pristine graphene (P-G) (consisting of 14 hydrogen atoms and 30 carbon atoms) (Figure 1(a)) and Ag-doped graphene (Ag-G) (consisting of 14 hydrogen atoms, 29 carbon atoms and 1 Ag atom) (Figure 1(b)), considering a nanosheet size of 3×3 supercell, where the outermost carbon atoms of both the structures were hydrogen-passivated to counter the dangling bonds. In order to obtain the Ag-doped graphene sheet structure (i.e. the Ag-G structure), a carbon vacancy was created at first into the graphene sheet, and then the Ag atom (as a dopant) was kept close at the top of the empty/vacant position, following which the structure was geometrically optimized. After the optimization, the Ag atom formed three single covalent bonds with its three neighbouring carbon atoms (Ag-C bonds), which is clearly visible in Figure 1(b).

The design, modeling and simulation of the molecular and materials properties of the thin films were carried out using the density functional theory (DFT) as the modeling methodology tool, employing Gaussian 09W and GaussView 6.0 platforms. DFT is a computational method through which the electronic properties and structure of many-electron systems are being investigated using functionals of electron density. In this present study, 3-21G was selected as the basis set for the calculations in Gaussian 09 platform due to the fact that the smaller basis sets like 3-21G yields similar results like the larger basis sets for comparatively smaller to standard (mediocre) dimensional structure like the one we

have designed here (i.e., 3×3 structure of graphene sheet with formaldehyde molecule), thereby the target was to reduce the computational cost (via using optimum basis set) during simulation, else the computational cost would arise noticeably due to the usage of larger basis set.

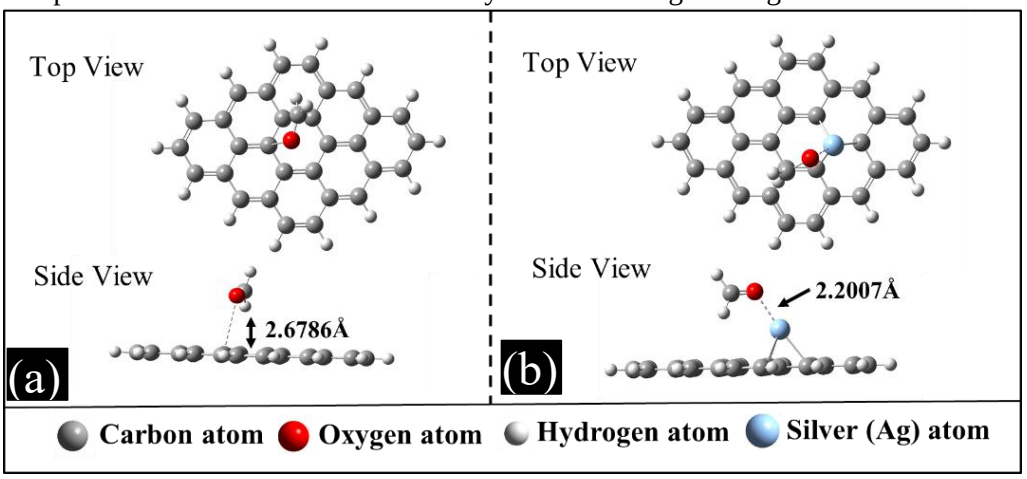

Figure 1. Optimized Structure of (a) Case-I, and (b) Case-II Configurations.

Along with the DFT method and 3-21G basis set, the PBEPBE (named after Perdew-Burke-Ernzerhof) functional was also used. Additionally, SCF=XQC keyword and initial guess of Extended Huckel were selected. Band Structure of both systems were plotted using DMol^3 software under Materials Studio packages using GGA-PBE approximations. For both Case-I and Case-II, the adsorption energies were calculated from the equation given below:

$$E_{Adsorption} = E_{Formaldehyde-Sensor} - E_{Formaldehyde} - E_{Sensor} \quad (1)$$

here, $E_{Adsorption}$ stands for the adsorption energy of Case-I or Case-II system (individually), $E_{Formaldehyde-Sensor}$ means the electronic energy of formaldehyde with P-G, or formaldehyde with Ag-G after optimization, $E_{Formaldehyde}$ means the electronic energy of formaldehyde after optimization, and E_{Sensor} means the electronic energy of P-G or Ag-G after optimization.

RESULTS AND DISCUSSION

Adsorption of Formaldehyde on Sensing Materials (P-G System and Ag-G System)

Frontier Molecular Orbitals (FMOs) Analysis:

The three-dimensional plots of molecular orbitals accompanied by their corresponding energy values have been shown for Case-I in Figure 2, and for Case-II in Figure 3, respectively. The FMOs, consisting of the HOMO and LUMO, give information related to the kinetic stability and chemical reactiveness. The portions where HOMOs are concentrated have a greater tendency to donate electrons whereas, the portions where LUMOs are concentrated are eager to accept electrons. In the HOMO-LUMO plot, red and green colours represented the positive and negative phases, respectively [12-14]. For Case-I, the total number of electrons was even, so restricted type functional was selected in Gaussian, leading to the formation of only alpha orbitals, which can be seen in Figure 2. On the other hand, due to odd number of electrons in Case-II, unrestricted type functional was imposed, so both the alpha orbital (which has up-spin electrons), and the beta orbital (which has down-spin electrons) were formed, which can be found in Figure 3. The key observations made from these figures are that, in Figure 2, the HOMO and LUMO were concentrated on the sensing material except the atom near the centre position (i.e. near the binding site), and not on the formaldehyde molecule. Whereas, in Figure 3, the HOMO and LUMO were found to be concentrated mostly on the sensing material including the atoms near the centre position (i.e. near the binding site), and also on the formaldehyde molecule. From Table 1, it is clear that the HOMO-LUMO gap decreased in Case-II (0.2732 eV for alpha orbital, and 0.8901 eV for beta orbital) than in Case-I (1.3352 eV for alpha orbital) facilitating easier electron transfer from HOMO to LUMO resulting in higher reactivity [12].

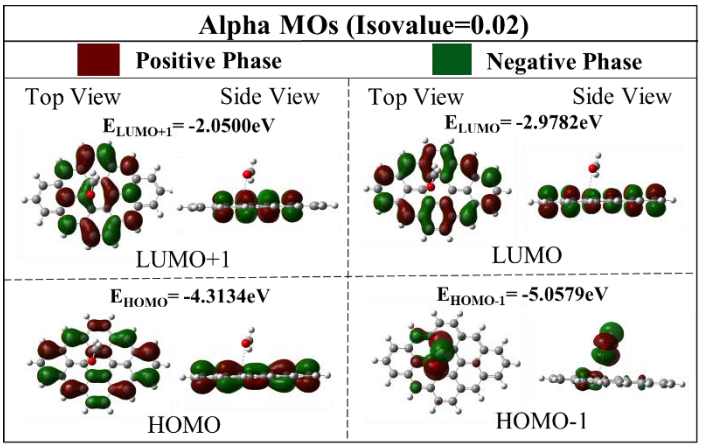

Figure 2. Alpha Molecular Orbitals of Case-I System with Top View as well as Side View.

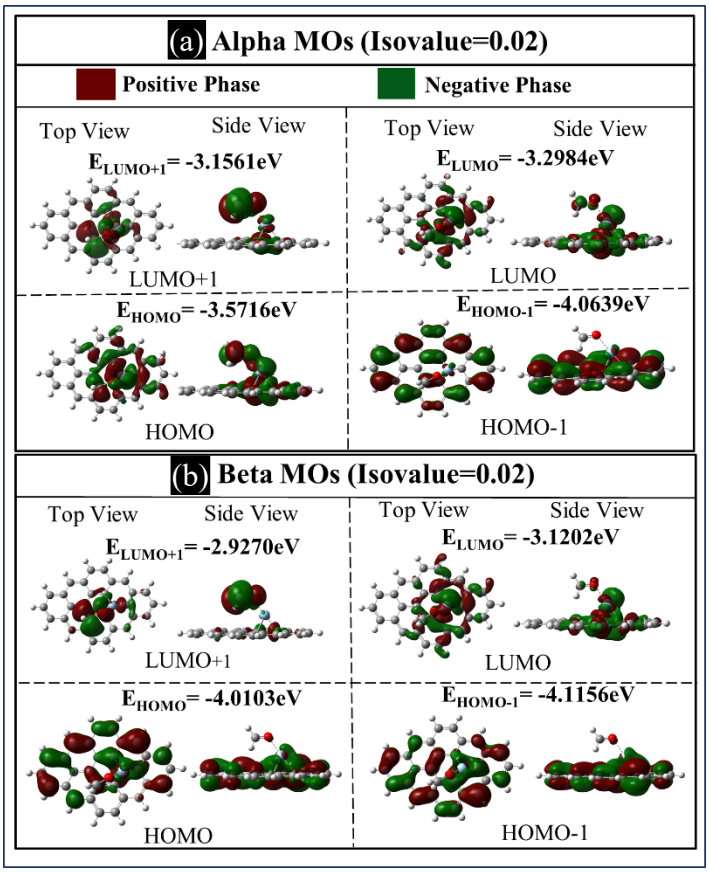

Figure 3. (a) Alpha Molecular Orbital, and (b) Beta Molecular Orbital of Case-II System with Top View as well as Side View.

Table 1. Orbital Energy and HOMO-LUMO Band Gap Calculation of Case-I, and Case-II Systems.

Case-I Configuration		**Case-II Configuration**		
	Alpha orbital (eV)		***Alpha orbital (eV)***	***Beta orbital (eV)***
E_{HOMO}	-4.3134	E_{HOMO}	-3.5716	-4.0103
E_{LUMO}	-2.9782	E_{LUMO}	-3.2984	-3.1202
E_{HOMO-1}	-5.0579	E_{HOMO-1}	-4.0639	-4.1156
E_{LUMO+1}	-2.0500	E_{LUMO+1}	-3.1561	-2.9270
$E_{HOMO - LUMO\ gap}$	1.3352	$E_{HOMO - LUMO\ gap}$	0.2732	0.8901

Electrostatic Potential (ESP) Analysis:

ESP is a property used to visualize the areas of positive and negative charges in the structure by means of colour coding [14]. In the colour coding, red denotes region of lesser electrostatic potential, green denotes neutral region and blue denotes the region of higher electrostatic potential. ESP was plotted for both Case-I and Case-II by using an isovalue of 0.0004. From Figure 4(a) (where the range was taken from -5.855e-2 eV to 2.755e-2 eV), it can be said that the density of green colour along the surfaces is more, which made those surfaces neutral; whereas, the outermost hydrogens were deep blue, which made them a target for nucleophilic attack. In the same figure (i.e. from Figure 4(a)), it can be easily observed that the red colour was present in a very small amount at only the binding site of the graphene sheet, and formaldehyde molecule for P-G system, which reduced the possibility of electrophilic attack to a great extent. On the other hand, from Figure 4(b) (where the range was taken from -9.250e-3 eV to 2.250e-2 eV), it can be seen that the red colour dominated the top surface, assisting in electrophilic attack in those regions [12-15]. It is well known that an atom or a molecule with a tendency to accept electrons would undergo electrophilic attack. The oxygen atom of the formaldehyde molecule, having more electronegativity than its neighboring carbon and hydrogen atoms, would get larger surface area for the electrophilic attack on the surface of Ag-G system, which means greater possibility of adsorption taking place. Thus, adsorption of the formaldehyde molecule on the Ag-G system would be more favourable than the adsorption on the P-G system.

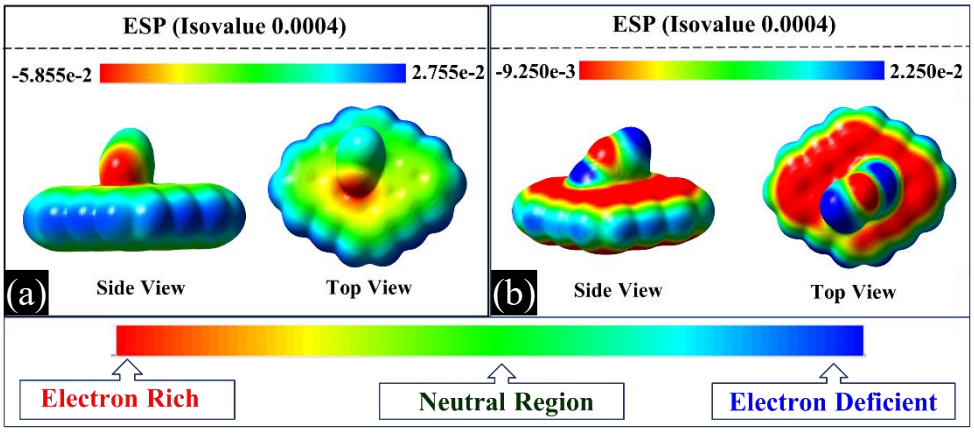

Figure 4. Electrostatic Potential Plot of (a) Case-I, and (b) Case-II Systems.

Mulliken Charge Analysis:

In Table 2, the charges on every atom for Case-I and Case-II systems are shown. After careful observation, it was found that in Case-II, the charge on the oxygen atom of formaldehyde was more negative than in Case-I, because in Case-II, the electronegative oxygen got attached to the more electropositive Ag atom, whereas in Case-I, the oxygen formed a bond with the C44 atom. Additionally, due to the presence of Ag atom (whose charge was 0.66687e) in Case-II, the amount of negative charges on the C7, C12 and C13 increased from (-0.01681e to -0.07779e), (0.00252e to -0.08121e), and (-0.00004e to -0.09332e), respectively. The C45 atom bonded with the oxygen atom (of formaldehyde molecule) via double bond in Case-I had the positive charge (0.0153e); whereas, the C44 atom bonded with the oxygen via double bond in Case-II had the negative charge (-0.00803e), which was compensated by more positive charges in the H46 (0.24871e), and H47 (0.21176e) atoms in Case-II than H47 (0.18211e) and H48 (0.15256e) atoms in Case-I. In more detail, the charge on oxygen atom of the formaldehyde molecule in Case-I was -0.34807e, and in Case-II, it was -0.36466e. The charge on the oxygen atom clearly got more negative upon the introduction of Ag atom in Case-II. Evidently, the charge transfer was more in Case-II. It is well known that higher amount of charge transfer indicates higher interaction between the molecules, which further imply that better adsorption has been taking place in second case [16-18]. So, the higher amount of charge transfer directly correlates with the better sensing performance of the sensing material.

Table 2. Mulliken Charge Analysis of Case-I, and Case-II Systems.

Case-I *Sys.		Case-II Sys.		Case-I Sys.		Case-II Sys.	
Atoms	****Mull. Ch. (e)***	***Atoms***	***Mull. Ch. (e)***	***Atoms***	***Mull. Ch. (e)***	***Atoms***	***Mull.Ch. (e)***
H33	0.20129	H33	0.20020	C2	-0.00838	C2	0.02046
C28	-0.19110	C28	-0.20831	C1	-0.00176	C1	-0.01178
C16	-0.19688	C16	-0.18438	H42	0.19037	H42	0.18771
H38	0.19522	H38	0.19491	H19	0.19101	H19	0.17630
C14	0.00305	C14	-0.06618	C18	-0.20262	C18	-0.18275
C15	-0.20588	C15	-0.18352	C20	0.00884	C20	-0.07873
H39	0.19014	H39	0.17664	C25	-0.19741	C25	-0.20225
C10	-0.00521	C10	-0.06569	H43	0.19528	H43	0.18911
C9	-0.191	C9	-0.17722	H37	0.19749	H37	0.1965
H40	0.19775	H40	0.20129	C30	-0.18456	C30	-0.17658
C8	-0.18988	C8	-0.20427	C31	-0.18544	C31	-0.20184
H41	0.19774	H41	0.19753	H36	0.19715	H36	0.19505
H32	0.19651	H32	0.19866	C21	0.00715	C21	0.01065
C29	-0.19560	C29	-0.18431	C22	-0.20462	C22	-0.20765
C17	0.00528	C17	-0.07809	H23	0.19099	H23	0.18557
C13	-0.00004	C13	-0.09332	C24	0.00323	C24	-0.00575
C44	0.01312	Ag48	0.66587	C26	-0.19659	C26	-0.20080
C7	-0.01681	C7	-0.07779	H35	0.19623	H35	0.19093
C5	-0.20619	C5	-0.21378	C27	-0.19137	C27	-0.19434
C6	0.00257	C6	-0.00874	H34	0.20129	H34	0.19525
C4	0.00201	C4	-0.00411	C45	0.0153	C44	-0.00803
C12	0.00252	C12	-0.08121	O46	-0.34807	O45	-0.36466
C3	-0.01215	C3	-0.09653	H47	0.18211	H46	0.24871
C11	-0.00463	C11	-0.08050	H48	0.15256	H47	0.21176

**Sys=system/configuration, *Mull. Ch.=Mulliken Charge*

Density of States (DOS) and Band Structure Analysis:

DOS spectrum gives insight into the number of states that are available for electrons to occupy at that specific energy level, which also means that if DOS value at the energy level is zero then there are no states left unoccupied at that energy level [19-20]. The DOS spectrum of Case-I is given in Figure 5(a), and that of Case-II is shown in Figure 5(b), respectively. By comparing both the figures, it can be seen that the height of the peaks seemed to be reduced for Case-II than for Case-I, which implied reduced contributions in the DOS spectrum due to more electron-transitions from valence band to conduction band. This is also in line with the previous observation that the HOMO-LUMO gap decreased in Case-

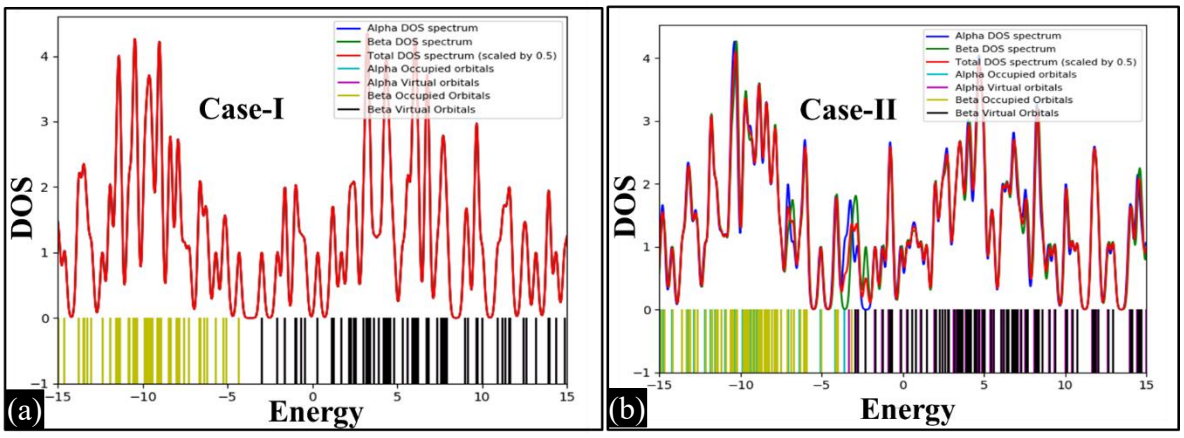

Figure 5. Density of States (DOS) Spectrum of (a) Case-I System, and (b) Case-II System.

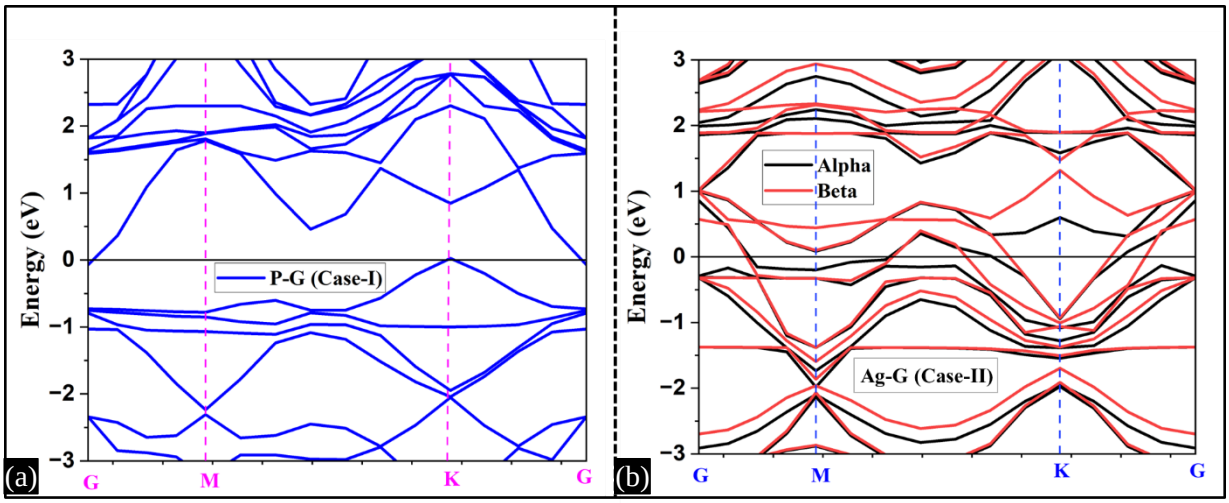

Figure 6. Band Structure of (a) Case-I System, and (b) Case-II System.

II in comparison to Case-I. The band structure of the Case-I system and Case-II system were plotted using different high symmetry points such as G, M, and K. In both the figures of band structure, as depicted in Figure 6(a) and Figure 6(b), there was an overlapping of valence band maxima and conduction band minima, which confirmed the semi-metallic nature of the graphene sheet.

Adsorption Energy and Binding Distance:

Adsorption energy calculated from the process is one of the major parameters on which the effectiveness of the sensing material depends. Good adsorption is supported by negative adsorption energy; whereas, positive adsorption energy means there were some errors in the computation [21-22]. The adsorption energies accompanied by the respective binding distances have been slated in Table 3 for further comparison. From the table, it can be observed that the adsorption energies for both Case-I and Case-II came negative, but the magnitude was seen to be higher in Case-II, which backs its higher

Table 3. Adsorption Energy and Corresponding Binding Distance of Case-I and Case-II Systems.

Adsorbed System	$*E_{Sensor}$ (in Hartree)	$*E_{Formaldehyde}$ (in Hartree)	$*E_{Formaldehyde\text{-}Sensor}$ (in Hartree)	$*E_{Adsorption}$ (in eV)	*Binding Distance (Å)
HCHO@P-Gs (Case-I)	-1143.965092	-113.729320	-1257.696459	-0.0557	2.6786
HCHO@Ag-Gs (Case-II)	-6281.374062	-113.729320	-6395.261504	-4.3026	2.2007

$*E_{Sensor}$: Sensing material, $*E_{Formaldehyde}$: Gas Adsorbed, $*E_{Formaldehyde\text{-}Sensor}$: Sensing Material with Gas Adsorbed, $*E_{Adsorption}$: Adsorption Energy (1 Hartree = 27.2107 eV)

Table 4. Comparison of the Sensing Parameters (Adsorption Energies and Binding Distances) between Different Metal-Doped Graphene based Structures for Formaldehyde Detection.

Different Doped-Graphene System	Adsorption Energy (in eV)	Binding Distance (Å)	References
Silicon-doped	-0.769	1.722	[26]
Aluminum-doped	-1.262	1.858	[26]
Chromium-doped	-1.215	1.960	[26]
Manganese-doped	-1.025	1.859	[26]
Gold-doped	-0.748	2.111	[26]
Titanium-doped	-1.84	2.030	[27]
Nickel-doped	-3.03	2.137	[28]
Palladium-doped	-3.07	2.408	[28]
Platinum-doped	-3.21	2.340	[28]
Silver-doped	-4.3026	2.2007	[This work]

stability than Case-I [23-25]. This also verifies the reverse trend seen in the binding distance, where a lesser value was found for Case-II owing to the stronger molecular interaction between the formaldehyde and Ag-doped graphene. Table 4 elaborately presents a comparison between the major results derived from our present work for Ag-doped graphene sheet along with the existing results (already published in different literatures) by other research groups considering other metal-doped graphene sheets cases. After observing the data present in Table 4, it is evident that the magnitude of adsorption energy is considerably higher for Ag-doped graphene sheet than the other reported cases, which further validates our simulation findings regarding the better sensing performance in Case-II compared to that of Case-I.

CONCLUSION

The potential application of Ag-doped graphene as a formaldehyde sensor has been analyzed in this current investigation. The value of the band gap calculated from the HOMO-LUMO plot was found to be lesser in Case-II (for both alpha orbitals and beta orbitals) than in Case-I. The adsorption energy value, which holds the key for determining effective sensing, was observed to be significantly higher in Case-II in comparison to Case-I. After optimization, the binding distance from the formaldehyde to the P-G sheet in Case-I was 2.6786Å; whereas, the binding distance from the formaldehyde to the Ag-G sheet in Case-II was found to be 2.2007Å. This result implied that formaldehyde came approximately 1.21 times closer to the sensing material in Case-II. Other parameters like DOS spectrum and band structure were also plotted to look into the nature of the nanostructures. Thus, the outcomes of our study make it evident that Ag-decorated graphene nanosheet can be used for high-performance application which provides better sensing performance than the pristine graphene, when it comes to formaldehyde sensing.

Acknowledgement

The authors thankfully acknowledge the Department of ECE, IEM, Kolkata. The authors also sincerely acknowledge Mr. Indrajit Maity, Department of EE, Indian Institute of Technology (IIT) Bombay for providing support in this research work.

REFERENCES

1. Badran HM, Eid KM, Al-Nadary HO, Ammar HY. Beryllium oxide nano-cage as sorbent and sensor for formaldehyde gas: DFT-D3 calculations. *Journal of Molecular Liquids*. 2023 Sep 1; 385: 122430.
2. Wang Z, Huang Z, Yu J, Shao X, Peng W, Yu J, Jiang Y. Growth of Ag/g-C_3N_4 nanocomposites on nickel foam to enhance photocatalytic degradation of formaldehyde under visible light. *Journal of Environmental Sciences.* 2024 Mar 1; 137: 432-442.
3. Zhang Y, Qiu X, Sun L, Yan Q, Luck RL, Liu H. A two-photon fluorogenic probe based on a coumarin schiff base for formaldehyde detection in living cells. *Spectrochimica Acta Part A: Molecular and Biomolecular Spectroscopy.* 2022 Jun 5; 274: 121074.
4. Shanmugasundaram A, Manorama SV, Kim DS, Jeong YJ, Lee DW. Toward Point-of-Care chronic disease Management: Biomarker detection in exhaled breath using an E-Nose sensor based on rGO/SnO_2 superstructures. *Chemical Engineering Journal*. 2022 Nov 15; 448: 137736.
5. Düzenli D. A comparative density functional study of hydrogen peroxide adsorption and activation on the graphene surface doped with N, B, S, Pd, Pt, Au, Ag, and Cu atoms. *The Journal of Physical Chemistry C*. 2016 Sep 15; 120(36): 20149-20157.
6. Singla M, Jaggi N. Enhanced hydrogen gas adsorption properties of B, N, and Au co-doped graphene in o-, m-, and p-configurations: DFT study. *Diamond and Related Materials*. 2022 Aug 1; 127: 109173.
7. Singh KK. A DFT studies on absorbing and sensing possibilities of glucose on graphene surface doped with Ag, Au, Cu, Ni & Pt atoms. *Biosensors and Bioelectronics: X*. 2023 May 1; 13: 100287.
8. Zhang X, Huang R, Gui Y, Zeng H. Gas sensing analysis of Ag-decorated graphene for sulfur hexafluoride decomposition products based on the density functional theory. *Sensors*. 2016 Nov 1; 16(11): 1830.

9. Yang L, Xiao W, Wang J, Li X, Wang L. Formaldehyde gas sensing properties of transition metal-doped graphene: a first-principles study. *Journal of Materials Science*. 2021 Jul; 56(21): 12256-12269.
10. Li Q, Liu Y, Chen D, Miao J, Zhi X, Deng S, Lin S, Jin H, Cui D. Nitrogen dioxide gas sensor based on Ag-doped graphene: a first-principle study. *Chemosensors*. 2021 Aug 14; 9(8): 227.
11. Singla M, Jaggi N. DFT analysis of hydrogen gas adsorption properties on Ag doped graphene. Materials Today: Proceedings. 2022 Jan 1; 66: 2104-2108.
12. Maity I, Nagasawa H, Tsuru T, Bhattacharyya P. Correlation between ammonia selectivity and temperature dependent functional group tuning of GO. *IEEE Transactions on Nanotechnology*. 2020 Dec 18; 20: 129-136.
13. Maity I, Ghosh K, Rahaman H, Bhattacharyya P. Tuning of electronic properties of edge oxidized armchair graphene nanoribbon by the variation of oxygen amounts and positions. *Journal of Materials Science: Materials in Electronics*. 2017 Jun; 28: 9039-9047.
14. Mahmood A, Akram T, de Lima EB. Syntheses, spectroscopic investigation and electronic properties of two sulfonamide derivatives: a combined experimental and quantum chemical approach. *Journal of Molecular Structure*. 2016 Mar 15; 1108: 496-507.
15. Maity I, Acharyya D, Huang K, Chung P, Ho M, Bhattacharyya P. A comparative study on performance improvement of ZnO nanotubes-based alcohol sensor devices by Pd and rGO hybridization. *IEEE Transactions on Electron Devices.* 2018 Jun 29; 65(8): 3528-3534.
16. Wang J, Zhou Q, Xu L, Gao X, Zeng W. Gas sensing mechanism of dissolved gases in transformer oil on Ag–MoS_2 monolayer: A DFT study. *Physica E: Low-dimensional Systems and Nanostructures*. 2020 Apr 1; 118:113947.
17. Liao N, Zhou H, Zheng B, Xue W. Silicon oxycarbide-derived carbon as potential NO_2 gas sensor: a first principles' study. *IEEE Electron Device Letters*. 2018 Sep 11; 39(11): 1760-1763.
18. Ren J, Kong W, Ni J. The potential application of BAs for a gas sensor for detecting SO_2 gas molecule: a DFT study. *Nanoscale Research Letters*. 2019 Dec; 14(1): 133.
19. Maity I, Bhattacharyya P. Room temperature acetone sensing performance of rGO-ZnO nanotubes binary hybrid structure. *Sensor Letters.* 2019 Jun 1; 17(6): 417-422.
20. Fatima Q, Zhang H, Haidry AA, Hussain R, Alshgari RA, Mohammad S. Elucidating the optoelectronic properties Ag, Au and Pd doped graphene oxide using a DFT approach. *Diamond and Related Materials*. 2024 Jun 1; 146: 111151.
21. Maity I, Ghosh K, Rahaman H, Bhattacharyya P. Selectivity tuning of graphene oxide based reliable gas sensor devices by tailoring the oxygen functional groups: A DFT study-based approach. *IEEE Transactions on Device and Materials Reliability*. 2017 Oct 25; 17(4): 738-745.
22. Mohammadi MD, Abdullah HY, Qadir KW, Suvitha A. Theoretical investigation of intermolecular interactions between CNT, SiCNT and SiCGeNT nanomaterials with vinyl chloride molecule: a DFT, NBO, NCI, and QTAIM study. *Diamond and Related Materials*. 2023 Jan 1; 131: 109602.
23. Maity I. Cadence Virtuoso based circuit simulation of universal logic gates: A board tutorial. *RP Cur. Tr. Eng. Tech.* 2024 Jan; 3: 1–7.
24. Verma CS, Shukla N, Bose P. Study of surface morphology and elemental investigation of chemically deposited mixed based photoconducting (Cd_x-Pb_y-Zn_z)S films. *RP Materials: Proceedings*. 2024 Jan; 3(1): 1–6.
25. Patel D, Mishra A. Hybrid sustainable nanomaterials using for nanofluids of advance applications and challenges of future scope, *RP Materials: Proceedings*. 2023 Sept; 2(1): 11–19.
26. Liu XY, Zhang JM. Formaldehyde molecule adsorbed on doped graphene: a first-principles study. *Applied Surface Science*. 2014 Feb 28; 293: 216-219.
27. Zhang HP, Luo XG, Lin XY, Lu X, Leng Y, Song HT. Density functional theory calculations on the adsorption of formaldehyde and other harmful gases on pure, Ti-doped, or N-doped graphene sheets. *Applied Surface Science*. 2013 Oct 15; 283: 559-565.
28. Li Y, Xu Y, Li X. The sensing mechanism of HCHO gas sensor based on transition metal doped graphene: Insights from DFT study. *Sensors and Actuators A: Physical*. 2022 May 1; 338: 113460.

